Contents lists available at ScienceDirect

Chemical Engineering Research and Design

journal homepage: www.elsevier.com/locate/cherd

Turbulent flow of shear-thinning liquids in stirred tanks—The effects of Reynolds number and flow index

Bart C.H. Venneker[1], *Jos J. Derksen*[2], *Harry E.A. Van den Akker*[*]

Department of Multi-Scale Physics, Delft University of Technology, Kramers Laboratorium voor Fysische Technologie, Prins Bernhardlaan 6, 2628 BW Delft, The Netherlands

ABSTRACT

LDA measurements are reported on the turbulent velocity fields in vessels agitated by a Rushton turbine and containing Newtonian as well as non-Newtonian, shear-thinning fluids. Ten different liquids were investigated, with flow indices varying from 1.00 down to 0.56. Experiments were performed in three vessel sizes, viz. 28.6, 44.1, and 62.7 cm in diameter, at various impeller speeds. The main issue of the paper is the question whether or not, and if so to what extent, turbulent flow of shear-thinning fluids differs from that of Newtonian liquids, or – in other words – whether and when turbulent flow of shear-thinning liquids exhibits Reynolds number similarity.

The experimental data presented comprise profiles of the mean velocity components and the rms fluctuating velocity components as a function of the radial position in the tank at the height of the impeller disc as well as similar profiles in the impeller outflow near to the impeller tip. The effects – if any – of both Reynolds number and flow index on these profiles are assessed.

Fit equations are presented for the various profiles in the various liquids. These fit equations are claimed to be valid throughout the ranges of Reynolds numbers and flow indices covered by the experiments presented. The idea is that these fit equations may be used to validate Computational Fluid Dynamics (CFD) simulations of the Reynolds Averaged Navier–Stokes (RANS) type for agitated shear-thinning liquids, even for liquids and conditions not investigated in this study as long as falling within the Reynolds number and flow index ranges investigated.

Keywords: Stirred tank; LDA; Turbulence; Shear-thinning

1. Introduction

The use of non-Newtonian liquids in process industry and in daily life is widely spread. Commonly used foods such as yogurt, sauces and soups, and emulsions like paint and latex all exhibit non-Newtonian characteristics. In domestic applications, these liquids seldom are in a turbulent motion; in the food, bio and paint industry, however, turbulent flow of these fluids occurs quite often.

As an example, several manufacturing processes start with a liquid being Newtonian and – because of the large scale of the equipment and the low liquid viscosity – flowing in the turbulent regime. During the process, however, the rheological behaviour of the liquid may change gradually and become more and more non-Newtonian, either because of chemical reactions taking place (polymerisation, fermentation) or because of additives (emulsions). Usually, viscosity increases during the process. In many cases, however, due to the large scale of the equipment the flow may remain largely turbulent, moving into the transitional regime just locally.

In order to obtain a sufficiently high yield of a product with reproducible properties, it is important that reactants are brought into an intimate contact with each other. The stirred vessel is one of the pieces of process equipment used to this purpose. An impeller is used for mixing the reactants and for creating a large contact area. Changing to a rheologically different liquid may affect optimal operating conditions and optimal mixing systems.

[*] *Corresponding author*. Tel.: +31 15 2785000.
E-mail address: h.e.a.vandenakker@tudelft.nl (H.E.A. Van den Akker).
Received 14 December 2008; Received in revised form 17 September 2009; Accepted 4 January 2010
[1] Present address: Stork Thermeq, P.O. Box 33, 7550AA Hengelo, The Netherlands.
[2] Present address: Department of Chemical & Materials Engineering, University of Alberta, Edmonton, Canada.
0263-8762/$ – see front matter
doi:10.1016/j.cherd.2010.01.002

Nomenclature

C	impeller clearance (m)
C_U, etc.	fit parameter in velocity correlations
d^2	squared difference in rank
D	impeller diameter (m)
H	tank height (m)
k_s	Metzner–Otto constant
K	fluid consistency (kg s^{n-2} m^{-1})
m_U, etc.	fit parameter in velocity correlations
M	number of data points
n	flow index
N	impeller rotational speed (s^{-1})
Q	radial volumetric discharge rate (m^3 s^{-1})
r	radial co-ordinate (m)
r_s	correlation coefficient
R	impeller radius (m)
R_0	dimensionless radius at which velocity changes sign
s	distance between impeller tip and measurement point (m)
t	coefficient from Student's t-distribution
T	tank diameter (m)
u	root mean square (rms) axial velocity (m s^{-1})
$\tilde{u}$	instantaneous velocity (m s^{-1})
u_0	fit parameter in rms axial velocity
U	mean axial velocity (m s^{-1})
v	root mean square (rms) radial velocity (m s^{-1})
V	mean radial velocity (m s^{-1})
V_{tip}	impeller tip velocity (m s^{-1})
w	width of impeller blade (m)
w	root mean square (rms) tangential velocity (m s^{-1})
W	mean tangential velocity (m s^{-1})
z	height co-ordinate (m)
z_0	dimensionless axial shift of the maximum velocity in impeller discharge

Greek letters

η	effective viscosity coefficient (Ns m^{-2})
$\dot{\gamma}$	shear rate (s^{-1})
λ	laser beam wave length (m)
ξ	correlating parameter in Eq. (2)
σ_V, σ_W	width parameter in impeller discharge correlations
τ_{res}	residence time of particle in measuring volume (s)
ω	weighing factor in velocity bias correction

Subscripts

wall	(interpolated) value at tank wall
0	value at z_0
1	value at impeller tip ($r/R = 1$)

Dimensionless groups

Fl	Flow number, Q/ND^3
Re	Reynolds number, $\rho N^{2-n} D^2 / K k_s^{n-1}$

In the early days of research on mixing of non-Newtonian liquids, most attention was devoted to the choice of the impeller and to overall mixing parameters such as power draw, mixing time and heat and mass transfer, in the laminar as well as in the turbulent regime. Much of this rather scarce work was already done in the 1960s, e.g. Skelland (1967), by exploiting techniques available at that time. Also Nouri and Whitelaw (1990) and Koutsakos and Nienow (1990) investigated the effect of non-Newtonian liquid properties on the mixing performance of stirred vessels. Very recently, Szoplik and Karcz (2008) experimentally studied mixing times for a non-Newtonian liquid agitated in an unbaffled vessel by an eccentric propeller – just to assess within the transitional flow regime the effects of impeller eccentricity, of impeller pumping mode, and of position of tracer dosage point. As a result, authoritative handbooks on (industrial) mixing (Tatterson, 1991; Paul et al., 2004) deal in full detail with the mixing of Newtonian liquids, while for non-Newtonian liquids only some overall mixing parameters are presented which may be useful for the engineering practice, but do not provide much guidance as to the underlying hydrodynamics.

Just a few papers on the hydrodynamics of non-Newtonian liquids in stirred vessels are available in the literature. Koutsakos and Nienow (1990) and Koutsakos et al. (1990) were among the very first to report on Laser-Doppler velocity measurements in non-Newtonian liquids. Most of these papers, however, are limited to the laminar, at most to the transitional flow regimes. This may be due to the complex nature of turbulence itself combined with the wide variety of non-Newtonian characteristics. Even in recent papers, due to, e.g. Fangary et al. (2000), Arratia et al. (2006), Adams and Barigou (2007) and Couerbe et al. (2008), the experimental and computational work presented is still restricted to the laminar flow regime, is mostly qualitative, and largely focuses on the occurrence of (pseudo-)caverns and on chaotic behaviour.

Nouri and Whitelaw (1990) studied the flow characteristics of stirred reactors with two Newtonian liquids and one non-Newtonian liquid stirred by both a Rushton turbine and a pitched-blade impeller. Their experiments do extend into the presumably turbulent flow regime; their results are largely qualitative however. In another paper, Nouri and Hockey (1998) focused on power number correlations. Recently, Nouri and Hockey (2008) presented an extensive set of detailed quantitative data on the mean and rms velocity characteristics for Newtonian and non-Newtonian liquids in a vessel equipped with a pitched-blade impeller; the framework and the data of their paper and of the current paper are rather complementary, already due to the mere difference in the impellers used in the experiments.

This paper addresses – for a vessel agitated by a Rushton turbine – the issue how long and when the non-Newtonian character of a liquid may still affect the flow field in a stirred vessel under conditions that one could characterise as probably (close to) turbulent. According to an old and common notion (Townsend, 1956; Hinze, 1959; Tennekes and Lumley, 1972), turbulent flows tend to be almost independent of viscosity (with the exception of the very smallest scales of motion which are viscosity dominated). This implies that the flow structure at sufficiently high Reynolds numbers, i.e. in the really turbulent regime, is similar – hence, this characteristic is called Reynolds number similarity. If a really turbulent flow is investigated, one usually finds that most mean-value features, when expressed non-dimensionally, are functions of the non-dimensional space co-ordinates only and no longer depend on the Reynolds number, i.e. on viscosity. The only condition is that the Reynolds number is sufficiently high. This Reynolds number similarity applies when just a length scale

and a velocity scale are sufficient to determine the structure of the turbulent flow field. The central issue of this paper is then whether and when, i.e. beyond which value of the (or a) Reynolds number, this common notion also applies to the (turbulent) motion of non-Newtonian liquids.

Since the late 1970s (Durst et al., 1976; Drain, 1980), Laser-Doppler Anemometry (LDA) has widely been used to characterise the flow structure in stirred vessels. Local measurements of velocity and turbulence characteristics in stirred vessels are predominantly carried out in the impeller stream. This is first of all due to the notion that the impeller stream largely determines the global circulation pattern, and hence mixing times. From a modelling point of view, the impeller stream region is crucial as well, since it was used in the 1970s and early 1980s for the establishment of semi-empirical jet models which would describe an essential feature of stirred vessels. Last but not least, in the early 1990s, measurement data in the impeller domain were used as (immersed) impeller boundary conditions for CFD simulations (Bakker, 1992; Bakker and Van den Akker, 1994; Venneker, 1999). Nowadays, sliding mesh techniques and multiple reference frame methods are widely used for RANS simulations, see e.g. Van den Akker (2006).

Measurements in other parts of the vessel have been performed by quite a few researchers, but are mostly presented in the form of vector plots to show the overall flow pattern, often in comparison with results from CFD simulations: see e.g. Bakker and Van den Akker (1994), for measurements with several impellers. It is difficult to obtain accurate quantitative experimental velocity data in the bulk of the tank from such vector plots.

Up to now, the majority of the published LDA data were measured in water with a variety of impeller types and vessel dimensions. Generally, the measurements for water in the fully turbulent regime show that the various velocity components at specific positions exhibit Reynolds number similarity indeed. As an example, Van der Molen and Van Maanen (1978) found that the mean radial velocity at the height of the impeller disc decays in the radial direction according to

$$\frac{V}{V_{tip}} = 0.85\left(\frac{r}{R}\right)^{-7/6} \tag{1}$$

This relationship provides a nice example of Reynolds number similarity, also denoted by the term asymptotic invariance (Tennekes and Lumley, 1972). In addition, this non-dimensional velocity is independent of the ratio of impeller to vessel diameter, D/T, up to 0.5, and of the scale of operation. Various similar correlations for other velocity components have been reported in the literature.

Another classical paper on LDA measurements in turbulent stirred vessels is that due to Wu and Patterson (1989). LDA data for liquids other than water are rather scarce however. Dyster et al. (1993) studied viscous Newtonian liquids, while Koutsakos and Nienow (1990) investigated shear-thinning liquids. According to Dyster et al. (1993), the effect viscosity, and hence Reynolds number, has on the above mean radial velocity profile, is described by

$$\frac{V}{V_{tip}} = 0.85\xi\left(\frac{r}{R}\right)^{-7/6} \tag{2}$$

where the relation between ξ and Re was given in a plot. It shows ξ increases with increasing Re and approaches a constant value, viz. 1.0, for $Re > 500$. Due to the relation between ξ and Re, the concept of Reynolds number similarity does not apply to all conditions at which Dyster et al. (1993) carried out their experiments. According to these authors, ξ is a good measure of the impact of viscosity on the flow number Fl which is defined as

$$Fl = \frac{Q}{ND^3} \tag{3}$$

where Q stands for the flow rate of fluid pumped by the impeller. For a Rushton turbine:

$$Q = \pi(D + 2s)\int_{-w/2}^{w/2} V dz \tag{4}$$

Dyster et al. (1993) found that both ξ and Fl had a constant value for $Re > 500$ (1.0 and 0.78, respectively). This finding implies that as far as the mean centre-line velocity is concerned, the turbulent flow in their vessels starts exhibiting Reynolds number similarity for $Re > 500$. The rms values of the radial velocity component at the impeller disc centre-line were also reported by Dyster et al. (1993) to be independent of Re for $Re > 500$; these rms values were fit by the following expression:

$$\frac{v}{V_{tip}} = 0.454 - 0.128\left(\frac{r}{R}\right) \tag{5}$$

The effective viscosity coefficients of the liquids used by Koutsakos and Nienow (1990) were found to obey a power–law relationship:

$$\eta = K\dot{\gamma}^{n-1} \tag{6}$$

with the flow index n ranging from 0.37 to 0.58. They found for all Reynolds numbers investigated that the pumping capacity of a Rushton impeller in shear-thinning liquids was always smaller than in Newtonian liquids. The relationship between Fl and Re was:

$$\begin{aligned} Fl &\propto Re \quad \text{for} \quad Re \leq 60 \\ Fl &\propto Re^{0.2} \quad \text{for} \quad Re \geq 60 \end{aligned} \tag{7}$$

This paper investigates a number of issues as to turbulent flows of non-Newtonian liquids in stirred vessels. The fundamental issue is addressed whether or not, and if so to what extent, in the fully turbulent regime the flow structure in a stirred vessel with shear-thinning liquids exhibits Reynolds number similarity, in other words is different from that with Newtonian liquids yes or no. The immediate question then is when the flow of a shear-thinning liquid is or starts becoming really or fully turbulent. With Newtonian liquids, the value of the Reynolds number is rather decisive. With shear-thinning liquids, however, this is less clear: first of all, the Reynolds number is defined differently because of the non-Newtonian viscosity; usually, the proposal due to Metzner and Otto (1957) is used for shear-thinning liquids: see furtheron in this paper – and, secondly, the shear rates and therefore also the effective viscosity of the liquid near to the impeller may be very different from the values at positions further remote from the impeller. As a result, it is not clear at which value of the Reynolds number defined according to Metzner and Otto (1957) the flow is really or fully turbulent and whether any statement about this applies to every position in the vessel simultaneously.

The approach pursued in this paper is to measure by means of LDA the phase-averaged velocity field at two typical positions in a vessel equipped with a Rushton turbine under conditions which may be supposed beforehand to be (close to) turbulent. The two typical positions are a horizontal plane at the level of the impeller disc – actually a horizontal line midway between two baffles – and a vertical plane in the outflow of the impeller directly at the impeller blade tip. (These two planes in the near vicinity of the impeller where turbulence intensity is maximum, are also relevant for many operations carried out in a stirred vessel.) Such measurements were carried out in two Newtonian liquids and in several shear-thinning liquids with varying flow index. The Reynolds number defined according to Metzner and Otto (1957) was also varied deliberately.

The non-Newtonian data presented in this paper are not only compared with own measurements in water, but also with data obtained in viscous Newtonian and non-Newtonian liquids by previous investigators. Secondly, the correlations proposed in the literature are re-examined and modified in order to fit our measured data as closely as possible. To this purpose, the number of points in each velocity profile was considerably increased compared to previous work.

The new correlations presented in this paper cover a rather wide range of Reynolds numbers – which for the most part are supposed to be representative of turbulent flow conditions – and are claimed to be valid for flow indices ranging from 0.64 up to 1.0. As a result, these correlations provide a useful data base for validating (future) CFD simulations of the (almost or largely) turbulent flow of shear-thinning liquids in stirred vessels. Even when velocity measurements have not been carried out for the exact flow indices and/or Reynolds numbers of interest, the new correlations provide guidance as to whether CFD simulations for such conditions are reliable or not. Since the new correlations have been derived on the basis of more data points than ever before, they are more accurate than previous ones.

After this introduction, details of the experimental set-up, the LDA measurements including data treatment, and the liquids used are discussed. The experimental results are presented, first for the mean velocity components and then for the total root-mean-square (rms) velocity components. The effects of the Reynolds number and the flow index on each velocity profile are analysed by the use of a non-parametric test. This outline is first applied to the so-called impeller disc height velocity data, and then to the impeller discharge data. Finally, conclusions as to our experimental findings are presented. In this paper, only the mean velocity components and the total rms velocity components are presented. This might be most useful for the purpose of validating CFD simulations of the Reynolds Averaged Navier–Stokes (RANS) type (Van den Akker, 2006). More detailed velocity data can be found in Venneker (1999).

2. Experimental

2.1. Stirred vessels

In this project, three geometrically scaled vessels were used with internal diameters of 0.286, 0.441, and 0.627 m, respectively. The vessels have the standard configuration (see Fig. 1 and Table 1), which means that most dimensions are some constant fraction of the tank diameter T. In all cases, a six-bladed disc turbine with diameter $D = T/3$ and clearance $C = D$ was used as the impeller. Only blade and disc thickness was not properly scaled. The vessels were filled with the working liquid up to a level $H = T$. At this level, there was a free surface. To minimise optical distortion, the flat bottomed perspex cylindrical vessels were placed inside square perspex containers. The space between the vessel and the container wall was in all cases filled with tap water.

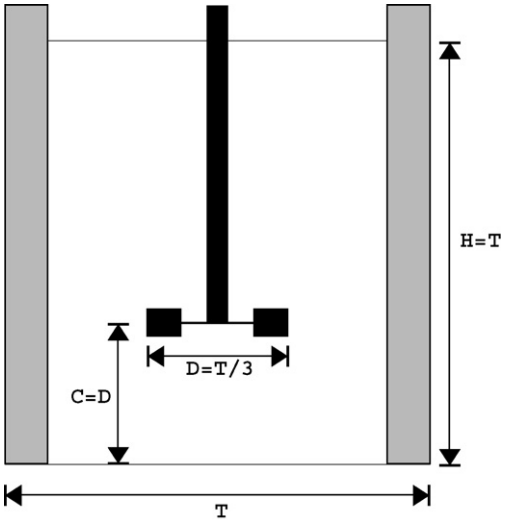

Fig. 1 – Geometry of the stirred vessel equipped with a Rushton turbine.

2.2. LDA set-up

A 4-W Spectra Physics Argon ion laser was used for all measurements. This laser produces light with three different wavelengths. In the experiments of this paper, only two of those were used: $\lambda = 514.5$ nm (green) and $\lambda = 488$ nm (blue). The laser light was coupled into a TSI Colorburst, model 9201, splitting the light into pairs of beams. By means of a Bragg cell, a fixed frequency shift of 40 MHz was added to one beam of each pair. The measuring volume in the liquid flow was approximately 1.5 mm long and about 0.1 mm wide. The measurements were taken in the *backward scatter mode*. The scattered light was guided to a TSI ColorLink model 9230, where the 40 MHz pre-shift was electronically downmixed to a user-set frequency shift (1 MHz in all cases).

The data were processed with an IFA750 (IFA = Intelligent Flow Analyzer). The signal was first filtered, in order to eliminate the pedestal and high frequency noise, and then amplified. After the analog Doppler signal having been digitised, bursts were detected based on signal-to-noise ratio. The

Table 1 – Vessel and impeller dimensions (in mm).

Vessel	T	286	441	627
Baffle width	b	29	45	61
Baffle thickness		5	7	6
Impeller	D	96	147	209
Blade height	w	19	29	42
Blade length	l_b	24	36	52
Blade thickness	d_b	2	2	3
Disc diameter		72	111	157
Disc thickness		2	2	3
Shaft diameter		19	28	38

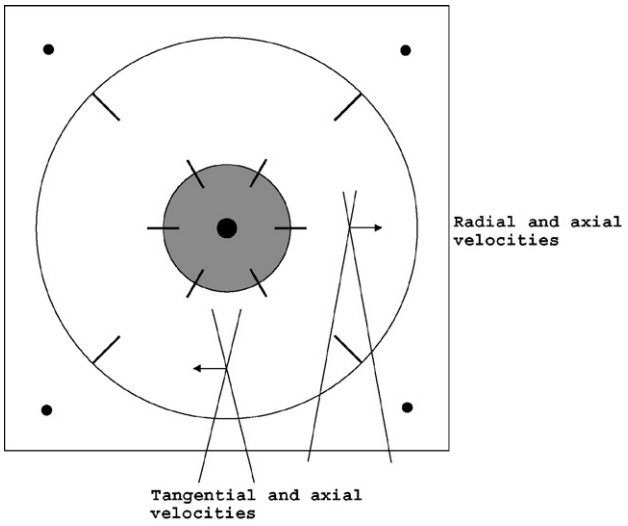

Fig. 2 – Orientation of the laser beams for the measurement of the three velocity components.

eventual Doppler frequency of the signal was performed by a double-clipped autocorrelator.

An oscilloscope was used to examine the quality of the Doppler bursts, and to measure the noise level. The software package FIND was used to set frequency pre-shift, threshold voltage, band-pass filter frequencies, validation mode, and acquisition mode. The actual determination of the velocities, based on the measured Doppler frequencies, and further post-processing of the data were done with a code developed in house.

2.3. *LDA measurements*

As stated previously, a 2D laser probe was used in all cases. The probe was fixed on an optical rail and a tripod in the case of the vessels 44.1 and 62.7 cm in diameter. The smallest vessel was placed in a 3D traversing system with the probe on a fixed position. The orientation of the laser beams for measuring tangential and radial velocities is shown in Fig. 2.

The total number of individual velocity measurements was about 20k points per measurement position and per velocity component. Most 2D measurements were taken in the random mode, i.e. all bursts with sufficient signal-to-noise ratio are taken into account. When the data rate was sufficiently high, also some measurements were taken in the coincidence mode (i.e. a velocity measurement is only validated if both channels simultaneously detect a burst). All measurements were performed in the single measurement per burst mode.

There are a number of biasing effects in LDA, the most important probably being *velocity bias*. During periods of relatively high absolute velocity, more scattering particles traverse the measuring volume. As a consequence, more particles with a high velocity than with a low velocity may be detected with a burst mode laser anemometer. As a result, simply arithmetical averaging of the individual realisation does not give the correct statistical moments of the velocity probability density function. Several methods have been proposed in the literature to correct for velocity bias, i.e. inverse-velocity weighing, residence time weighing, and time-between-data weighing. These methods were examined in Venneker (1999). The best method was found to be residence time weighing that corrects for particles with a low absolute velocity having a long residence time (τ_{res}) in the measuring volume. An estimate of τ_{res} is based on the burst length.

The mean flow quantities presented in this work are calculated by the following estimators:

$$U = \frac{\sum_{i=1}^{M} \tilde{u}_i \omega_i}{\sum_{i=1}^{M} \omega_i} \tag{8}$$

and

$$\overline{u^2} = \frac{\sum_{i=1}^{M} (\tilde{u}_i - U)^2 \omega_i}{\sum_{i=1}^{M} \omega_i} \tag{9}$$

with $\omega_i = \tau_{res,i}$ as the weighing factor, and M the number of individual velocity measurements.

Only the measurements of the profiles at the impeller disc height and the impeller discharge profiles are presented in this paper. The profiles comprise about 20 individual measurement positions and are all phase-averaged. More details can be found in Venneker (1999).

2.4. *Shear-thinning liquids*

The shear-thinning liquids used were prepared by dissolving polymers into water. The shear-thinning behaviour was controlled by means of the weight percentage of polymer added. Two different types of polymers were selected, based on reports in the literature (not experimentally verified by us) that they do not exhibit elastic behaviour. In addition, these two polymer solutions exhibit substantial shear-thinning properties at relatively low apparent viscosities.

The first polymer used is carboxy methyl cellulose (CMC) manufactured by Aqualon, trade name Blanose. The weight percentages CMC were in the range 0.1–0.2%. Lower weight percentages showed no clear shear-thinning, while with higher percentages the apparent viscosities were too high to reach the turbulent flow regime in the vessels used.

The second polymer used was Xanthan gum, manufactured by Kelco, trade name Keltrol RD. Solutions of this material are less transparent than the blanose solutions; as a matter of fact, this caused significant scattering of the laser beams at weight percentages higher than 0.1%. At the same weight percentage, however, the Xanthan solutions were more shear-thinning than the CMC solutions.

The rheograms of the solutions were well described by a power-law relationship, see Eq. (6). A summary of all values of K and n for the solutions presented in this paper, together with the vessel size in which they were investigated, is listed in Table 2.

3. Impeller disc height profiles

3.1. *Mean velocities*

3.1.1. *Results for water*

First, velocity data measured in water are presented and where possible compared with literature data. Throughout the text, the following notation is used: U and u for the axial velocity, V and v for the radial velocity, and W and w for the tangential

Table 2 – Rheological properties of the solutions.

Solution	wt%	$K \times 10^{-3}$ [kg s^{n-2} m^{-1}]	n [–]	T [cm]
Water	–	1.0	1.00	44.1 and 62.7
Glycerol	75	33.0	1.00	28.6
Blanose	0.1 (a)	31.6	0.77	28.6
	0.1 (b)	13.2	0.85	44.1 and 62.7
	0.2	119.4	0.68	28.6
Keltrol	0.045	9.5	0.80	62.7
	0.05 (a)	16.5	0.71	44.1
	0.05 (b)	23.6	0.68	44.1
	0.08	34.0	0.64	62.7
	0.10	74.8	0.56	44.1

velocity, where capitals denote mean velocities and regular symbols the root mean square (rms) values.

Fig. 3 shows data measured in the 44.1-cm tank, at an impeller speed of $N = 3.0$ rev/s, i.e. $Re = 65 \times 10^3$. Empirical correlations and measurements by other authors are also shown in this figure.

The solid lines drawn in this figure are fits to the data. They are based on the following equations:

Axial velocity:

$$\frac{U}{V_{tip}} = U_{wall} + (U_1 - U_{wall})\left(\frac{r}{R}\right)^{-m_U} \tanh^2\left[C_U\left(\frac{T}{D} - \frac{r}{R}\right)\right] \quad (10)$$

Radial velocity:

$$\frac{V}{V_{tip}} = V_1\left(\frac{r}{R}\right)^{-m_V} \tanh\left[C_V\left(\frac{T}{D} - \frac{r}{R}\right)\right] \quad (11)$$

Tangential velocity:

$$\frac{W}{V_{tip}} = \frac{1}{\frac{1}{W_1} + C_W \ln^2\left(\frac{r}{R}\right)} \quad (12)$$

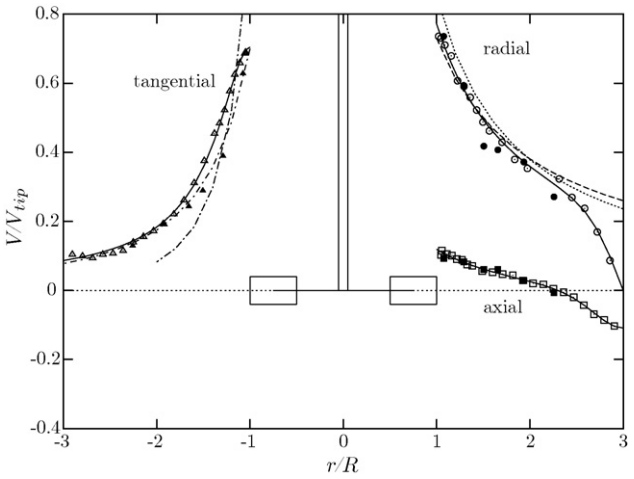

Fig. 3 – Profiles of the mean velocities in water at the impeller disc level. Open symbols: measurement data reported in this paper; solid lines: correlations presented in this paper (44.1 cm vessel; $Re = 65,000$); dotted line: correlation for V/V_{tip} due to Van der Molen and Van Maanen (1978); dashed line: correlation of V/V_{tip} due to Dyster et al. (1993); closed symbols: experimental data reported by Wu and Patterson (1989); dot-dash line: correlation of W/V_{tip} due to Lunden (1995); steep dot-dash line: correlation of W/V_{tip} due to Koutsakos and Nienow (1990).

In these equations, U_1, V_1, and W_1 denote the values of the velocity components at $r/R = 1.0$, for the axial, radial and tangential direction, respectively, made non-dimensional with V_{tip}. Further, U_{wall} is the extrapolated axial velocity at the wall, also made non-dimensional with V_{tip}, the parameter m in each equation is an exponent, and C_U, C_V, and C_W are scaling constants for the radial position.

The form of these formulae is purely descriptive, with no physical meaning. To some extent, Eqs. (10) and (11) remind of expressions found in the literature, such as Eqs. (1) and (2). These formulae, Eq. (12) in particular, were found by using the program TableCurve2D.[1] With this program it is possible to simultaneously fit thousands of fit equations to a data set. From the 'best-fit' equations the most simple one was selected, with polynomial equations being excluded.

The measurements of the mean *radial* velocity in water (see Fig. 3) show the expected profile: a decrease inversely proportional with r at $r/R = 1.0$ which levels off around $r/R = 2.0$, and decreases to zero at the wall. The agreement with previous correlations and measurements from literature is good for radial distances $r/R < 2.0$. Closer to the vessel wall, the decay is well described by our new correlation (11). The fit parameters in this case were set to $V_1 = 0.772$, $m_V = 1.10$, and $C_V = 2.99$. The tank over impeller diameter ratio, T/D was 3.0. Eq. (11) is an extended version of the Van der Molen–Van Maanen correlation, Eq. (1), and has the advantage that it can be used for vessels with different T/D-ratios. This has been tested (Venneker, 1999) for the data of Nouri et al. (1987) for three T/D ratios.

The *axial* velocity profile in water (see also Fig. 3) shows that the outflow from the impeller is slightly directed upwards. This is a known fact for stirred tanks in which the clearance between impeller and vessel bottom is usually smaller than half the liquid height (Yianneskis et al., 1987; Mishra and Joshi, 1993). Excellent agreement is found with the measurements due to Wu and Patterson (1989). No correlations for U/V_{tip} were found in the literature, but the data are well described by Eq. (10). The fit parameters were $U_{wall} = -0.109$, $U_1 = 0.119$, $m_U = 0.704$, and $C_U = 2.34$.

The *tangential* velocity profile in water (see also Fig. 3) shows a rapid decrease for non-dimensional radial distances between $r/R = 1$ and $r/R = 2$, and then levels off to a constant value of approximately $W/V_{tip} = 0.1$. The measured velocities close to the impeller are somewhat higher than those measured by Wu and Patterson (1989) and by Lunden (1995), but the overall trend is comparable. The correlation due to Koutsakos

[1] http://www.systat.com/products/TableCurve2D.

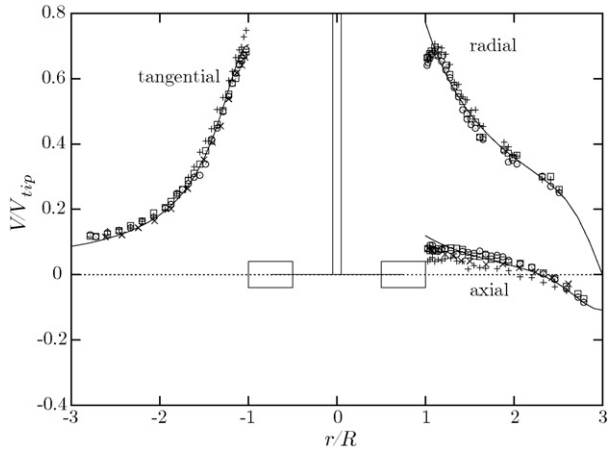

Fig. 4 – Reynolds effect on mean velocity profiles in 0.1% Blanose ($n = 0.85$); all data were measured in the 62.7-cm vessel except the data at $Re = 5,900$ which were measured in the 28.6-cm vessel. Measurements—+: $Re = 5,900$; ×: $Re = 15,000$; □: $Re = 16,900$; ⊙: $Re = 22,200$; solid lines: fit of water data obtained in the 44.1-cm vessel at $Re = 65,000$.

and Nienow (1990).

$$\frac{W}{V_{tip}} = 1.0\left(\frac{r}{R}\right)^{-3.6} \tag{13}$$

is quite different; this may be due to their data having been measured in the plane of a baffle. Our data in water are well described by Eq. (12) with $W_1 = 0.7045$ and $C_W = 8.40$.

3.1.2. *Reynolds number effect*

Although the experimental conditions with the shear-thinning liquids were such that the flow was at least in the transitional regime, the Reynolds number in each case may not have been sufficiently high to *a priori* exclude any effect of the Reynolds number on the flow profiles. Therefore, each fluid was studied at two impeller speeds at least. The Reynolds numbers for the experiments with the shear-thinning liquids were calculated according to the Metzner–Otto method (Metzner and Otto, 1957):

$$Re = \frac{\rho N^{2-n} D^2}{K k_s^{n-1}} \tag{14}$$

with $k_s = 11.5$ where the so-called Metzner–Otto constant k_s is the proportionality constant in the linear relationship between the average shear rate (in the laminar flow regime) and the impeller speed N. An obvious question is of course whether k_s still bears physical significance in calculating values of the Reynolds number for conditions in the transitional and turbulent flow regimes.

In Fig. 4, the measurements in 0.1 wt% Blanose, flow index $n = 0.85$, are shown as measured at four different impeller speeds. Also shown are the fitted curves for the experiments with water (see Fig. 3).

As far as the *tangential* velocity data in Fig. 4 are concerned, only the data at the lowest impeller speed (which probably are in the transitional regime) deviate from the data for the other three conditions which further almost perfectly coincide with the curve for water. This is also the case for the *radial* velocity, shown on the right-hand side of Fig. 4. The only difference between the Blanose solutions and water is the increase of V/V_{tip} just at the start of the radial outflow, i.e.

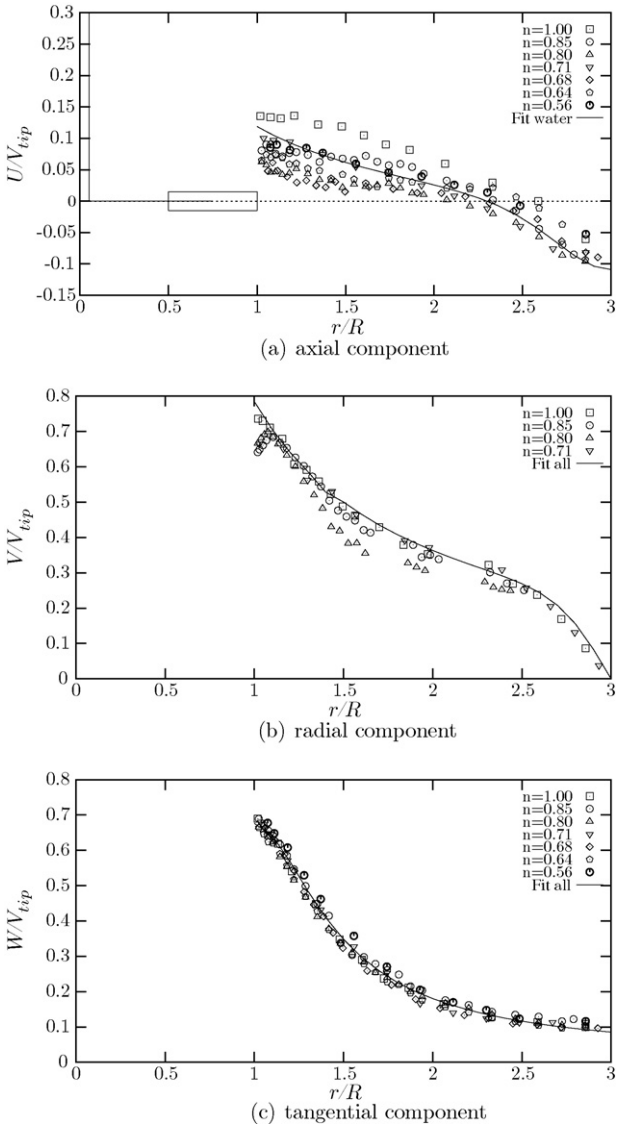

Fig. 5 – Radial profiles of the three mean velocity components at the impeller disc level for all fluids at their highest Reynolds number; solid line in (a) relates to water data in the 44.1-cm vessel (lower *Re*-number). (a) Axial component, (b) radial component, (c) tangential component.

between $r/R = 1.00$ and $r/R = 1.10$. These findings are indicative of the absence of any effect of *Re* on both the tangential and radial velocity profiles at least for the higher Reynolds numbers.

The *axial* velocity data, however, do exhibit an effect of *Re*. The data for the lower Reynolds numbers indicate that again the upward directed velocity components between $r/R = 1.0$ and $r/R = 2.0$ are smaller than those measured for water at $Re = 64,800$. Also the non-dimensional radial position where the axial velocity changes sign, denoted by the symbol R_0, shows a *Re*-dependency.

3.1.3. *Effect of the flow index*

A total of six different shear-thinning liquids were studied with flow indices ranging from 0.85 down to 0.56. In Fig. 5, the mean velocity components in each liquid are compared mutually and to measurements in water. Only the measurements at the highest Reynolds number for each liquid are in this figure. Fit parameters of Eqs. (10)–(12) for each experiment are given in Tables 3–5 for the axial, radial and tangential velocity

Table 3 – Results mean axial velocity fit (impeller disc height) with Eq. (10).

Solution	n [–]	T [cm]	N [rev/s]	Re	U_1	U_{wall}	m_U	C_U
Water	1.00	44.1	3.0	64.8×10^3	0.119	−0.109	0.704	2.34
Water	1.00	62.7	3.0	131.0×10^3	0.144	−0.061	0.376	1.60
0.1% Blanose (b)	0.85	62.7	1.2	5.9×10^3	0.0666	−0.0617	−0.196	0.794
0.1% Blanose (b)	0.85	44.1	5.0	15.0×10^3	0.0819	−0.0679	0.711	2.38
0.1% Blanose (b)	0.85	62.7	3.0	16.9×10^3	0.0842	−0.0856	0.251	1.70
0.1% Blanose (b)	0.85	62.7	3.8	22.2×10^3	0.0850	−0.101	0.182	1.71
0.045% Keltrol	0.80	62.7	1.5	12.2×10^3	0.0200	−0.0736	0.217	2.25
0.045% Keltrol	0.80	62.7	3.5	33.7×10^3	0.0569	−0.108	0.410	1.99
0.05% Keltrol (a)	0.71	44.1	2.0	6.5×10^3	0.0648	−0.0385	0.634	1.74
0.05% Keltrol (a)	0.71	44.1	4.1	16.4×10^3	0.110	−0.0905	0.493	1.40
0.05% Keltrol (b)	0.68	44.1	3.0	8.5×10^3	0.0395	−0.0777	0.438	3.02
0.05% Keltrol (b)	0.68	44.1	4.0	12.5×10^3	0.0512	−0.0952	0.466	2.78
0.08% Keltrol	0.64	62.7	1.5	5.4×10^3	0.0554	−0.0464	0.730	3.12
0.08% Keltrol	0.64	62.7	3.0	13.8×10^3	0.0736	−0.1376	0.395	4.41
0.10% Keltrol	0.56	44.1	4.1	6.4×10^3	0.0989	−0.0573	0.589	1.80

Table 4 – Results mean radial velocity fit (impeller disc height) with Eq. (11).

Solution	n [–]	T [cm]	N [rev/s]	Re	V_1	m_V	C_V
Water	1.00	44.1	3.0	64.8×10^3	0.772	1.10	2.99
0.1% Blanose (b)	0.85	62.7	1.2	5.9×10^3	0.853	1.22	3.62
0.1% Blanose (b)	0.85	62.7	3.0	16.9×10^3	0.797	1.17	5.95
0.1% Blanose (b)	0.85	62.7	3.8	22.2×10^3	0.789	1.22	5.70
0.045% Keltrol	0.80	62.7	3.5	33.7×10^3	0.775	1.41	11.6
0.05% Keltrol (a)	0.71	44.1	2.0	6.5×10^3	0.782	1.01	3.00
0.05% Keltrol (a)	0.71	44.1	4.0	15.9×10^3	0.708	0.89	2.50
All except 0.045% Keltrol	–	–	–	–	0.785	1.11	3.63
Glycerol	1.00	28.6	4.0	1.3×10^3	0.828	0.82	2.09
Glycerol	1.00	28.6	6.0	1.9×10^3	0.837	0.79	1.90
Glycerol	1.00	28.6	8.0	2.5×10^3	0.809	0.72	1.90
0.1% Blanose (a)	0.77	28.6	5.0	3.7×10^3	0.847	0.95	1.90
0.1% Blanose (a)	0.77	28.6	6.0	4.6×10^3	0.841	0.96	1.90
0.1% Blanose (a)	0.77	28.6	7.0	5.5×10^3	0.830	0.94	1.90
0.2% Blanose	0.68	28.6	4.0	1.0×10^3	0.780	0.91	1.90
0.2% Blanose	0.68	28.6	6.0	1.8×10^3	0.798	0.95	1.90
0.2% Blanose	0.68	28.6	8.0	2.6×10^3	0.834	0.91	1.90

component, respectively, and in the supplementary Excel-file. Keep in mind that these fit parameters are just the result of an optimisation procedure. As a result, they neither necessarily bear physical significance nor relate – at a first sight – consistently to Reynolds number and/or flow index. This will be addressed below in greater detail.

Starting with the *axial* velocity, Fig. 5(a), a whole band of data points is visible, with the measurements in water in the largest tank at the upper extreme. The solid line in the figure is the fitted profile for the water data in the 44.1-cm vessel. From this figure, and from the data shown in Fig. 4, it is not clear whether the variation in the data points is a Reynolds

Table 5 – Results mean tangential velocity fit (impeller disc height) with Eq. (12).

Solution	n [–]	T [cm]	N [rev/s]	Re	W_1	C_W
Water	1.00	44.1	3.0	64.8×10^3	0.705	8.40
Water	1.00	62.7	3.0	131.0×10^3	0.674	8.79
0.1% Blanose (b)	0.85	62.7	1.2	5.9×10^3	0.732	7.38
0.1% Blanose (b)	0.85	44.1	5.0	15.0×10^3	0.665	8.47
0.1% Blanose (b)	0.85	62.7	3.0	16.9×10^3	0.674	7.53
0.1% Blanose (b)	0.85	62.7	3.8	22.2×10^3	0.676	8.01
0.045% Keltrol	0.80	62.7	1.5	12.2×10^3	0.660	8.64
0.045% Keltrol	0.80	62.7	3.5	33.7×10^3	0.653	8.86
0.05% Keltrol (a)	0.71	44.1	2.0	6.5×10^3	0.655	8.78
0.05% Keltrol (a)	0.71	44.1	4.1	16.4×10^3	0.679	8.68
0.05% Keltrol (b)	0.68	44.1	3.0	8.5×10^3	0.687	9.10
0.05% Keltrol (b)	0.68	44.1	4.0	12.5×10^3	0.677	9.41
0.08% Keltrol	0.64	62.7	1.5	5.4×10^3	0.676	8.54
0.08% Keltrol	0.64	62.7	3.0	13.8×10^3	0.652	9.14
0.08% Keltrol	0.64	62.7	3.0	13.8×10^3	0.653	9.07
0.10% Keltrol	0.56	44.1	4.1	6.4×10^3	0.694	7.41
All	–	–	–	–	0.676	8.48

Table 6 – Example of non-parametric test with Spearman's rank-order correlation coefficient.

Re	n	U_1	R_{Re}	R_{U_1}	$(R_{Re}-\overline{R_{Re}})^2$	$(R_{U_1}-\overline{R_{U_1}})^2$	$(R_{Re}-\overline{R_{Re}})(R_{U_1}-\overline{R_{U_1}})$
64,800	1.00	0.119	14	14	36	36	36
131,000	1.00	0.143	15	15	49	49	49
5,900	0.85	0.047	2	3	36	25	30
15,000	0.85	0.082	9	10	1	4	2
16,900	0.85	0.083	10.5	10	6.25	4	5
22,200	0.85	0.084	12	10	16	4	8
12,200	0.80	0.020	6.5	1	2.25	49	10.5
33,700	0.80	0.057	13	5.5	25	6.25	−12.5
6,500	0.71	0.064	3.5	7	20.25	1	4.5
16,400	0.71	0.107	10.5	13	6.25	25	12.5
8,500	0.68	0.040	5	2	9	36	18
12,500	0.68	0.051	6.5	4	2.25	16	6
5,400	0.64	0.055	1	5.5	49	6.25	17.5
13,800	0.64	0.074	8	8	0	0	0
6,400	0.56	0.098	3.5	12	20.25	16	−18
			8	8	278.5	277.5	168.5

number effect only, or is also due to the shear-thinning nature of the liquids. Again, this issue will further be dealt with in the next section. The spread in the LDA data is also visible in the fit parameters given in Table 3. Along with the obvious spread in U_1 and U_{wall}, particularly the parameters indicating the slope, m_U, and the position with zero axial velocity, C_U, exhibit considerable variation.

As far as the *radial* velocity is concerned, comparing in Fig. 5(b) the profiles for $n = 1.00$, i.e. water, and the shear-thinning liquids shows two differences. First, the small maximum in V, just outside the impeller swept region, which is there for all polymer solutions but is absent in water (at higher Reynolds numbers), although only observed in the 62.7-cm vessel, where the relative spatial resolution of the measuring system was highest. Second, the sharper decay of V for radial distances larger than, say, $r/R = 1.2$ for $n = 0.80$ (0.045% Keltrol) which is probably due to relatively low data rates in this case.

Also shown in Fig. 5(b) is the fit with Eq. (11) of all experiments but the 0.045% Keltrol ($n = 0.8$). This line gives a very good representation of the velocity profile, although the local maximum around $r/R = 1.0$ is not included. For convenience, the proposed correlation Eq. (11) with the fitted parameters is repeated here:

$$\frac{V}{V_{tip}} = 0.785\left(\frac{r}{R}\right)^{-1.11}\tanh\left[3.63\left(\frac{T}{D}-\frac{r}{R}\right)\right] \tag{15}$$

the factor T/D having the value of 3 in all cases.

In Table 4, the parameters V_1 and m_V exhibit a small non-systematic variation only. The spread in C_V is much larger and may be due to the deviation between the correlation and the measurement data for the smaller radial distances.

Also given in Table 4 are the results of the fits for the smallest of the three vessels. These measurements were taken in the plane of a baffle; this explains why the parameters have values different from those in the two other vessels. Each profile for the small vessel is based on 6 data points only, whereas in the other vessels 15 to 20 data points are involved. Thus, in the smallest vessel, the profile is more sensitive to measuring errors and the profile is not that accurate as one would like. This is the reason why no overall fit was made for these cases.

The *tangential* velocity has been measured in all seven liquids, see Fig. 5(c). The spread is small and just due to uncertainties in the measurements. Consequently, the tangential velocity can be predicted by a single correlation for all fluids, see Table 5:

$$\frac{W}{V_{tip}} = \frac{1}{(1/0.676)+8.48\ln^2(r/R)} \tag{16}$$

3.2. *Spearman's rank-order correlation coefficient*

To investigate whether either the Reynolds number or the shear-thinning character of the solutions has the most dominant effect on the *axial* velocity profile, the profiles of all axial velocity measurements were analysed further. A non-parametric test was performed on three characteristic points of the profile: U_1 (the dimensionless axial velocity at the impeller tip), R_0 (the dimensionless radius at which the axial velocity changes sign), and U_{wall} (the extrapolated axial velocity at the vessel wall). A non-parametric test elucidates whether or not there is a significant monotonic relationship between two variables. A test is *non-parametric* since the dependent variable (U_1, R_0 or U_{wall}) is descriptive for the measured profile, while the relationship with the independent variable Re or n is not clear *a priori*.

The non-parametric test used exploits Spearman's rank-order correlation coefficient (Sheskin, 1997) which works with rank-order data. As indicated above, this method tests whether or not there is a significant monotonic increase/decrease in the data. A relationship between two variables is monotonically increasing, if an increase in the value of one variable is always accompanied by an increase in the value of the other variable. This test does not says anything about causality, because the increase in both variables may be caused by a third, unknown, variable. As the method works with rank-order data, the rank in the total data set is important rather than the actual increase of a variable. An example of this method is shown in Table 6.

In this example, the test is performed on the relationship between U_1 and Re. Let R_{Re} be the rank of Re_i among the other Re's, and R_{U_1} the rank of $U_{1,i}$ among the other U_1's . In the fourth column of Table 6, the rank of the independent variable Re is given, and in the fifth column the rank of the dependent variable U_1. As can be seen in the table, some entries are combined and get a common 'averaged' rank due to small differences in Re or U_1. The bottom row in these two columns presents the respective averaged ranks. The last three columns of the

Table 7 – Results non-parametric tests for the mean velocity fits (impeller disc height).

Profile	Parameter	$t_{.05}$	$t(n)$	$t(Re)$	Significant-n	Significant-Re
Axial velocity	U_1	1.77	1.38	2.75	no	yes
	U_{wall}	1.77	−0.53	−2.81	no	yes
	R_0	1.77	−0.72	0.13	no	no
Radial velocity	V_1	2.02	0.97	−1.13	no	no
	m_V	2.02	0.86	0.58	no	no
Tangential velocity	W_1	1.76	0.78	−0.64	no	no
	W_{wall}	1.76	1.70	−0.14	no	no

table contain the squared deviations from the averaged rank, and in the bottom row the sums of these squared deviations. The duplicate measurement of the tangential velocity in 0.08% Keltrol with $N = 3.0$ was used to estimate the error in the different parameters. The rank-order correlation coefficient, r_s, is defined as the linear correlation coefficient of the ranks, *viz.*

$$r_s = \frac{\sum(R_{Re} - \bar{R}_{Re})(R_{U_1} - \bar{R}_{U_1})}{\sqrt{\sum (R_{Re} - \bar{R}_{Re})^2}\sqrt{\sum (R_{U_1} - \bar{R}_{Re})^2}} \quad (17)$$

The absolute value of r_s is indicative of the strength of the relationship between the two variables. The significance of a nonzero value of r_s is tested by computing

$$t = \frac{r_s\sqrt{M-2}}{\sqrt{1-r_s^2}} \quad (18)$$

which is distributed as the Student's t-distribution with $M - 2$ degrees of freedom. A table of the Student's t-distribution reports the following critical value at the one-tailed 95% significance level: $t_{.05} = 1.771$. In Table 7, the values found for the Reynolds dependency of U_1 and U_{wall} are higher than this critical value however. Hence, the *axial* velocities near the impeller and near the vessel wall significantly depend on the Reynolds number. This is not the case for the position of R_0. On the basis of similar arguments, the flow index is found to have no significant effect at all on the axial velocity profile.

This is illustrated in Fig. 6 where the values of U_1 and also R_0 have been plotted against the Reynolds number (a) and the flow index (b). In spite of the scatter in the data, the increasing trend of U_1 with Re (open symbols) is evident. The reason for the scatter is probably due to experimental errors, such as positioning errors in the measuring volume of the laser beams. The results for the mean *radial* and *tangential* velocity are presented in Table 7 as well. Neither the Reynolds number nor the flow index seems to have an effect on the mean radial and mean tangential velocity profiles.

3.3. *RMS velocities*

In a stirred vessel, the rms velocity variations in the vicinity of the impeller of course comprise two contributions: a periodic, i.e. non-random component stemming from the impeller blade passage, and the truly (or really) turbulent fluctuations of the overall flow field. Rather than by performing phase resolved LDA measurements, the non-random fluctuations due to the passage of the impeller blades were extracted from the total velocity fluctuations by autocorrelating the velocity signal (Wu and Patterson, 1989). The impeller speed proves to be recovered accurately by using the latter method. In this paper, however, the total (= periodic + turbulent) rms velocity data are presented only, except in Table 8 where results for both the periodic and the truly turbulent contributions are presented.

As a common basis for comparing for the various liquids the velocity profiles in a horizontal plane at the level of the impeller disc, the following correlations are suggested

$$u_{tot}: \frac{u}{V_{tip}} = \frac{u_0}{((r/R) - R_0)^{m_u}}\left[1 - \exp\left(-\frac{((r/R) - R_0)^{1+m_u}}{C_u}\right)\right] \quad (19)$$

$$v_{tot}, w_{tot}: \quad \frac{u}{V_{tip}} = \frac{v_1 - v_\infty}{1 + [C_R \log(r/R)]^m} + v_\infty \quad (20)$$

which again are meant purely descriptive only.

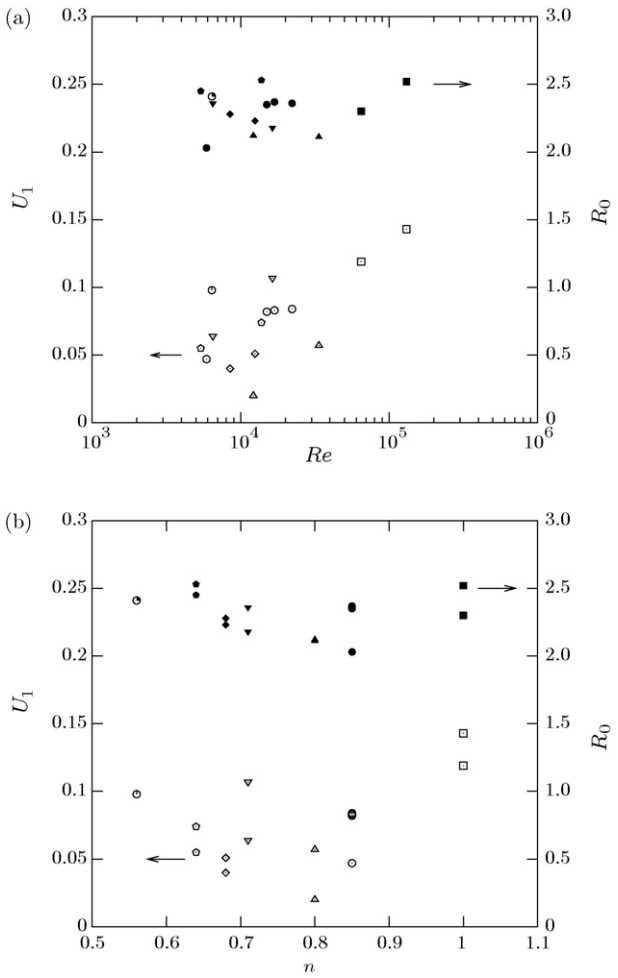

Fig. 6 – Dependence of U/V_{tip}-fit on Re (a) and n (b). Closed symbols: R_0, open symbols: U_1. Symbols refer to the same liquids as in Fig. 5.

Table 8 – Results non-parametric tests for the rms velocity fits (impeller disc height).

Profile	Parameter	$t_{.05}$	$t(n)$	$t(Re)$	Significant-n	Significant-Re
Total rms axial velocity	u_1	1.77	−0.81	1.06	no	no
	u_{max}	1.78	−0.12	0.67	no	no
	R_{max}	1.78	−0.08	−1.09	no	no
	u_{wall}	1.77	−0.16	0.56	no	no
Turb. rms axial velocity	u_1	1.77	−0.09	1.10	no	no
	u_{max}	1.77	0.84	−0.21	no	no
	R_{max}	1.77	−1.15	−1.10	no	no
	u_{wall}	1.77	1.01	0.04	no	no
Periodic rms axial velocity	u_1	1.77	−0.31	0.13	no	no
	u_{max}	1.78	0.89	2.25	no	yes
	R_{max}	1.80	−0.64	−2.15	no	yes
Total rms radial velocity	v_1	2.02	2.39	0.41	yes	no
	v_{wall}	2.13	−0.63	0.20	no	no
Turb. rms radial velocity	v_1	2.02	0.09	0.80	no	no
	v_{max}	2.02	1.38	3.41	no	yes
	R_{max}	2.02	0.17	−1.07	no	no
	v_{wall}	2.02	0.77	2.14	no	yes
Periodic rms radial velocity	v_1	2.13	1.06	0.18	no	no
	R_0	2.02	1.10	−0.93	no	no
Total rms tangential velocity	w_1	1.76	2.69	4.22	yes	yes
	w_{wall}	1.76	1.38	1.97	no	yes
Turb. rms tangential velocity	w_1	1.78	−0.89	−0.33	no	no
	w_{max}	1.76	2.22	2.68	yes	yes
	R_{max}	1.76	−0.25	−0.29	no	no
	w_{wall}	1.76	1.54	2.78	no	yes
Periodic rms tangential velocity	w_1	1.76	1.47	2.21	no	yes
	R_0	1.76	0.64	1.27	no	no

3.3.1. *Results with water*

First, the velocity profiles measured in water (see Fig. 7) are discussed and compared with some literature data.

The *axial* total rms velocities in the impeller disc plane show an initial increase up to the radial distance $r/R \approx 1.35$. This is mainly caused by the return-to-isotropy effect of vanishing pressure fluctuations due to the pressure difference over the impeller blades. Both the *radial* and the *tangential* total rms velocities in the impeller disc plane initially have a constant value; they decrease sharply until they level off when approaching the vessel wall. The initial constant level may be explained by the increase in the truly turbulent fluctuations and the simultaneous decrease in the periodic component caused by the disintegration of the trailing vortices.

Only the *radial* rms velocities are in line with literature data, while for the other two components the measured data are higher than those reported by Wu and Patterson (1989). The higher resolution of our measurements, however, results in a more detailed representation of the flow field. So far, for example, the profile for the total radial rms velocity was described with a linear correlation, viz. Eq. (5) due to Dyster et al. (1993), although some of Dyster's data do show a flat section near to the impeller. The conclusion from our measurements is that a straight line is too rough an approximation indeed.

3.3.2. *Effect of the shear-thinning solutions*

Fig. 8 presents the measured rms velocities for each of the seven fluids used in the 44.1 and 62.7 cm vessel. Only the data at the highest Reynolds numbers are shown.

Eqs. (19) and (20) were used to fit the measured total rms velocities for each of the seven shear-thinning solutions. The fits for the separate rms contributions, i.e. for the periodic contributions due to the blade passages and for the truly turbulent contributions, are available in Excel-files and can be obtained from the corresponding author.

Here, too, the question is whether or not, and if so to what extent, the rms profiles, i.e. the turbulent character and the turbulent properties of the flow, are sensitive to the Reynolds number and/or the flow index. To this end, for some characteristic points of these profiles (cf. section 3.2), a non-parametric test was performed as well. The results are given in Table 8, not only for the total rms component but also for the separate periodic and the truly turbulent contributions. In case all characteristics points did not exhibit a significant variation with either the flow index or the Reynolds number, an overall fit was made to the data points of all liquids investigated. In some cases, clear outliers had been removed with a view to the non-parametric test.

Fig. 8(a) shows the *axial* (total) rms velocity profile at the impeller disc level. Although there is some scatter in the data with the different solutions, u can be correlated well with a single equation for all liquids, in agreement with the results presented in Table 8. This equation runs as

$$\frac{u}{V_{tip}} = \frac{0.225}{((r/R) - 0.794)^{1.10}} \left[1 - \exp\left(-\frac{((r/R) - 0.794)^{1+1.10}}{0.273}\right)\right] \quad (21)$$

and is shown in the figure as the drawn line. For radial positions ($r/R < 1.2$), the measurements are better correlated with:

$$\frac{u}{V_{tip}} = 0.207 + 1.88\left(\frac{r}{R} - 1\right)^{2.14} \quad (22)$$

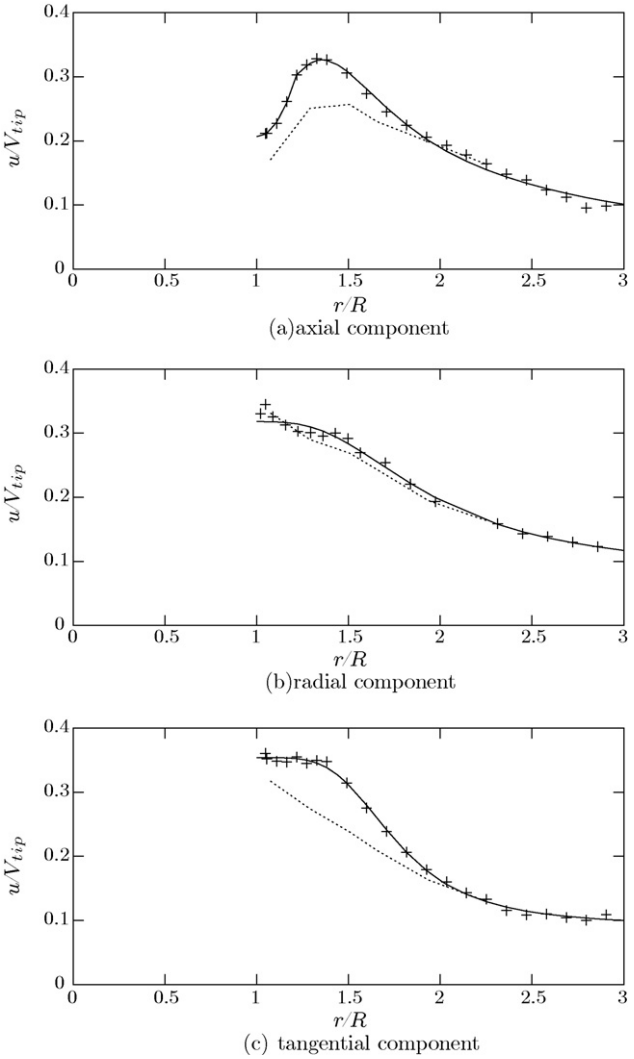

Fig. 7 – Radial profiles of the rms velocities at the impeller disc level for water. Symbols: measurements from this work; Solid lines: correlations from this work; small dashed line: experimental data by Wu and Patterson (1989). (a) Axial component, (b) radial component, (c) tangential component.

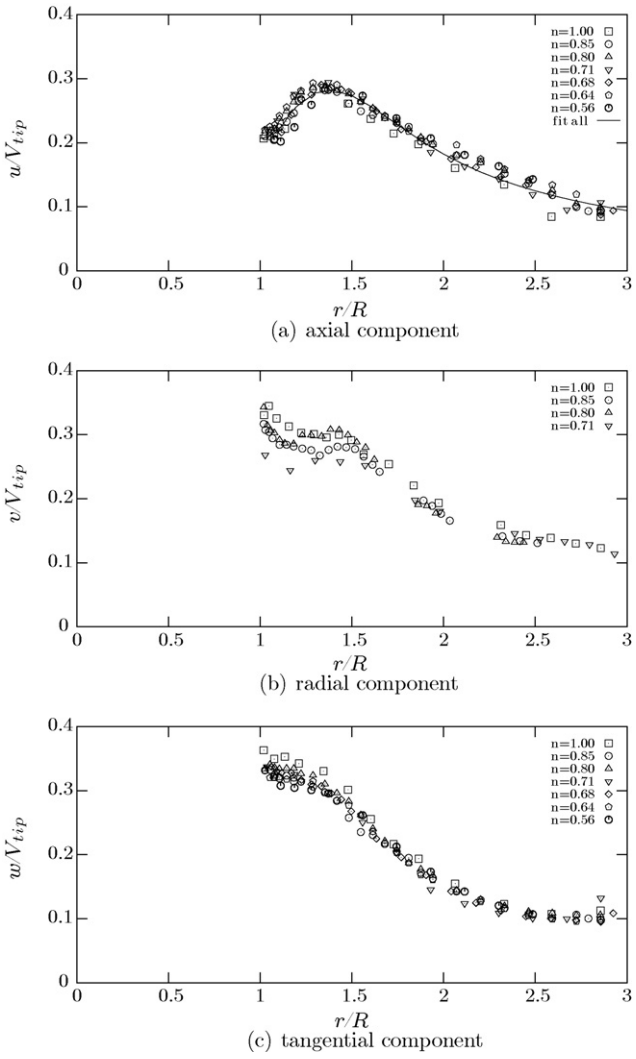

Fig. 8 – Radial profiles of the rms velocities at the impeller disc level for all fluids at their highest Reynolds number. (a) Axial component, (b) radial component, (c) tangential component.

In contrast to the findings for the mean axial velocity, no Re-dependency was found.

The spread in the *radial* rms velocity in Fig. 8(b) is a bit higher and the Spearman test (see Table 8) reveals that close to the impeller v_{tot} depends on the flow index.

Finally, the *tangential* rms velocity data are presented in Fig. 8(c). Close to the impeller tip, there is a rather large spread in the data points, and w/V_{tip} is a function of the flow index, with the highest value for $n = 1.00$ and the lowest for $n = 0.56$, which is the 0.10% Keltrol solution. Further away from the impeller, the data band narrows, and the data appear to collapse on a single curve. Because of the many data points, it is not clear from the figure what the exact trend in the data is, but from Table 8 we conclude that also the Reynolds number has some effect. As a matter of fact, both trends are significant, the relationship between *Re* and $w_{(r/R)=1}$ being the strongest.

It should be noted that in our experiments *Re* and *n* were not varied independently, because the apparent viscosity increased with decreasing flow index. Experiments with the highest Reynolds number were therefore carried out with $n = 1.00$, and experiments with the lowest Reynolds number with the lowest flow index. More experiments with (more) viscous Newtonian fluids and/or shear-thinning fluids in a larger vessel may be needed to investigate these trends in more detail.

4. The impeller discharge

4.1. *Velocity profiles*

The outflow of the revolving impeller, or the pumping capacity, is an important property, as this outflow imposes the revolving and circulatory flow pattern throughout the vessel and by doing so has an impact on, e.g. circulation time, residence time (distribution) and solids suspension. Of course, also in computational simulations this outflow is a highly relevant property, in terms of both mass source and momentum source. Therefore, the velocity profiles at the tip (measured at the dimensionless radial position R^*) and along the height of the blade will now be presented and discussed.

4.1.1. *Radial velocity*

In Fig. 9(b) these profiles are presented for three different fluids. The line drawn in Fig. 9(b) is the fit for 0.1% Blanose with

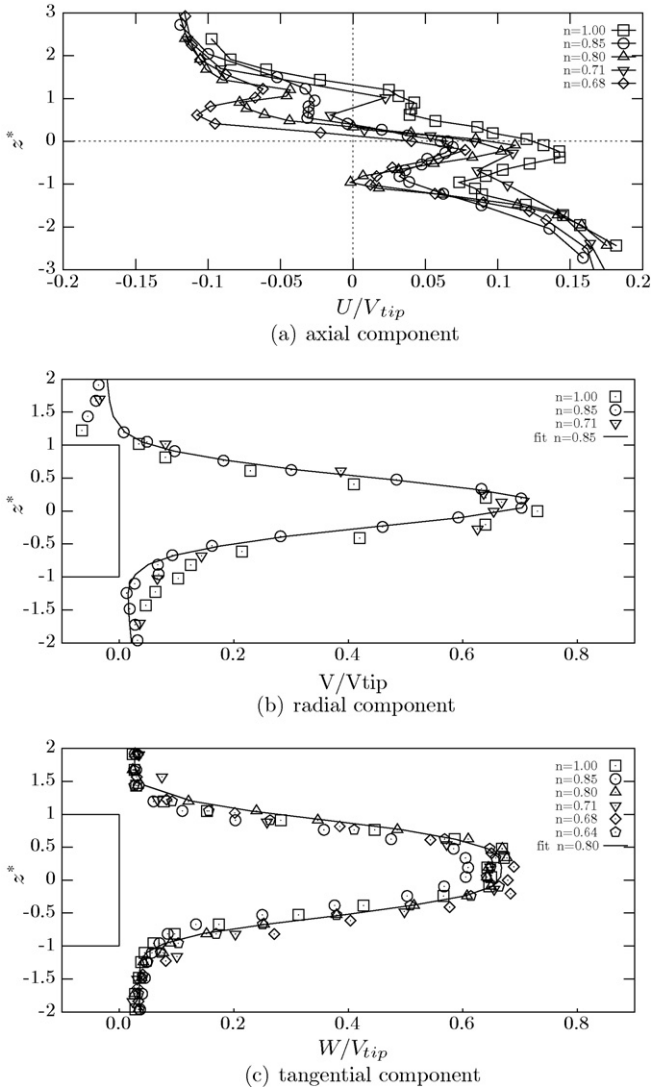

Fig. 9 – Impeller discharge profiles at their highest Reynolds numbers in the impeller discharge domain. (a) Axial component, (b) radial component, (c) tangential component.

the following correlation:

$$\frac{V}{V_{tip}} = \frac{V_1}{R^*} \exp[-C \cdot |z^* - z_0|^m] + b \cdot z^* \quad (23)$$

in which $z^* = 2z/w$, with w denoting the blade height. The results of the fits for all experiments with this correlation are given in Table 9.

4.1.2. *Tangential velocity*

The outflow profile of the tangential velocity is shown in Fig. 9(c) for various liquids. The width (with respect to the blade height) of this profile is larger than that of the radial velocity profile. The explanation is that, because of the no-slip condition at the impeller surface, the liquid is forced to revolve with the impeller over most part of the blade height. Hence, the profile is much flatter around $2z/w = 0.0$. The fit correlation for the mean tangential velocity is very similar to Eq. (23):

$$\frac{W}{V_{tip}} = \frac{W_1}{R^{*2}} \exp[-C \cdot |z^* - z_0|^m] + w_\infty + b \cdot z^* \quad (24)$$

in which the first term on the right-hand side represents the characteristic bell-shaped outflow profile with a maximum at $z^* = z_0$. The two last terms account for the small slope that is present above and below the impeller.

In the figure, and also in Table 10, some variation in the width and the maximum of the profile is visible. Part of this effect is due to the fact that not all profiles were measured on exactly the same non-dimensional position; this, however, should be compensated for by the factor $(r/R)^{-2}$ in Eq. (24). Whether or not there are trends in the width and the maximum of the profiles was again investigated by means of a non-parametric test. The results of these tests are given in Table 11.

The values of t suggest that the variation of the width is significantly related to the flow index only. Apparently, the entrainment of fluid is higher in shear-thinning fluids than in Newtonian fluids. The spread in the maximum velocity is not significant and is probably just due to experimental errors.

4.1.3. *Axial velocity*

The measured mean axial velocity along the impeller blade exhibits a rather oscillating profile and no satisfactory correlation fitting the experimental data was found. In Fig. 9(a), the measured data are shown for the highest Reynolds number for each of the fluids. The lines are only meant to guide the eye. In order to detect a possible effect of the Reynolds number and/or the flow index, again a non-parametric test was performed on the (interpolated) experimental data at $z^* = -2, -1, 0, +1, +2$. Results for the measurements in the $T = 44.1$ cm and $T = 62.7$ cm vessels are given in Table 11. These data are indicative of a rather small effect of both Reynolds number and flow index, the differences between the various profiles being in the order of a few cm/s only.

Table 9 – Results mean radial velocity fit (impeller outflow) with Eq. (23).

Solution	n [–]	T [cm]	N	Re	R^*	V_1	C	m	z_0	b
Glycerol	1.00	28.6	4.0	1300	1.042	0.827	4.32	2.13	0.05	−0.008
Glycerol	1.00	28.6	6.0	2000	1.042	0.840	3.55	1.93	0.05	−0.010
Glycerol	1.00	28.6	8.0	2600	1.042	0.818	3.51	1.95	0.04	−0.010
Water	1.00	44.1	3.0	64,800	1.048	0.781	2.74	1.74	0.01	−0.033
0.1% Blanose (b)	0.85	62.7	2.0	10,600	1.019	0.737	2.86	1.76	0.07	−0.006
0.1% Blanose (b)	0.85	62.7	3.8	22,200	1.019	0.741	3.13	1.87	0.14	−0.011
0.1% Blanose (a)	0.77	28.6	5.0	3700	1.042	0.832	4.19	2.01	0.05	−0.010
0.1% Blanose (a)	0.77	28.6	6.0	4600	1.042	0.830	3.66	1.88	0.05	−0.010
0.1% Blanose (a)	0.77	28.6	7.0	5500	1.042	0.819	3.37	1.84	0.05	−0.010
0.05% Keltrol	0.71	44.1	4.1	16,400	1.041	0.700	2.38	2.04	0.12	−0.009
0.2% Blanose	0.68	28.6	4.0	1000	1.042	0.754	5.08	2.18	0.04	−0.007
0.2% Blanose	0.68	28.6	6.0	1700	1.042	0.788	5.01	2.20	0.05	−0.008
0.2% Blanose	0.68	28.6	8.0	2600	1.042	0.806	4.89	2.14	0.04	−0.009

Table 10 – Results mean tangential velocity fit (impeller outflow) with Eq. (24).

Solution	n [–]	T [cm]	N	Re	R^*	W_1	C	m	z_0	w_∞	b
Water	1.00	44.1	3.0	64,800	1.048	0.773	2.26	2.58	−0.01	0.019	0.006
Water	1.00	62.7	2.5	109,200	1.019	0.662	2.50	3.19	0.19	0.031	−0.001
0.1% Blanose (b)	0.85	62.7	2.0	10,600	1.019	0.625	2.79	3.05	0.25	0.043	−0.001
0.1% Blanose (b)	0.85	44.1	5.0	15,000	1.027	0.637	2.58	2.73	0.07	0.035	0.001
0.1% Blanose (b)	0.85	62.7	3.8	22,200	1.019	0.596	2.94	2.98	0.18	0.038	−0.002
0.045% Keltrol	0.80	62.7	1.5	12,200	1.019	0.680	1.64	2.84	0.15	0.039	−0.004
0.045% Keltrol	0.80	62.7	3.0	28,000	1.019	0.662	1.76	3.19	0.18	0.031	−0.003
0.05% Keltrol	0.71	44.1	4.1	16,400	1.020	0.660	1.76	2.89	0.07	0.030	0.004
0.05% Keltrol	0.68	44.1	3.0	8500	1.048	0.726	1.34	2.57	0.04	0.036	0.000
0.05% Keltrol	0.68	44.1	4.0	12,500	1.048	0.726	1.52	2.84	0.07	0.031	0.002
0.08% Keltrol	0.64	62.7	1.5	5,400	1.019	0.662	2.16	3.02	0.10	0.049	−0.002
0.08% Keltrol	0.64	62.7	3.0	13,800	1.019	0.656	2.04	3.06	0.14	0.036	−0.003

Table 11 – Results non-parametric tests for the mean velocity fits (impeller outflow).

Profile	Parameter	$t_{.05}$	$t(n)$	$t(Re)$	Significant-n	Significant-Re
Axial velocity	$U@z^* = -2$	1.943	1.22	3.16	no	yes
	$U@z^* = -1$	1.943	1.36	1.53	no	no
	$U@z^* = 0$	1.943	2.70	4.93	yes	yes
	$U@z^* = +1$	1.943	3.17	3.18	yes	yes
	$U@z^* = +2$	1.943	2.36	2.79	yes	yes
Radial velocity	$V@R^* = 1, z^* = z_0$	1.796	1.15	−1.70	no	no
	z_0	1.796	−0.53	1.27	no	no
	Width @ $V = 0.2$	1.796	2.22	4.40	yes	yes
	Fl	1.796	2.63	1.18	yes	no
Tangential velocity	$W@R^* = 1, z^* = z_0$	1.812	−0.86	−0.52	no	no
	z_0	1.812	0.66	0.34	no	no
	Width @ $W = 0.2$	1.812	−2.43	−1.25	yes	no

4.2. *Flow number*

As already mentioned in the introduction of this paper, the Flow number Fl is a good indicator of the pumping capacity of an impeller. The measurements of Fl in Newtonian fluids (Dyster et al., 1993) and in shear-thinning liquids (Koutsakos and Nienow, 1990) show a Reynolds number dependence of Fl in the laminar and transitional regime. The calculated values of Fl reported in both papers are shown in Fig. 10.

For both types of fluids, two regimes can be distinguished: a sharp increase of Fl with increasing Re in the laminar regime

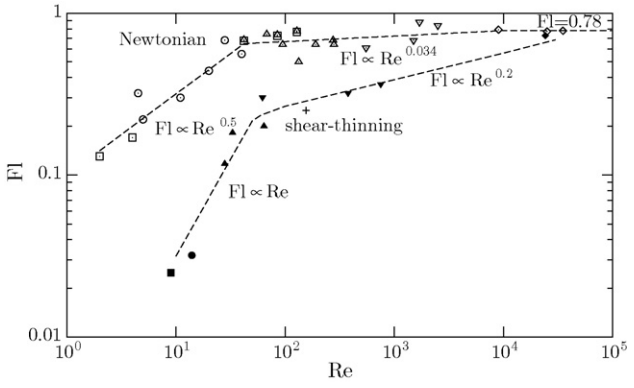

Fig. 10 – Flow number Fl as a function of the Reynolds number, literature data. □: glucose solution; ⊙: 100% glycerol; △: glycerol solution; ▽: PEG solution; ◇: water; ■: 2% Natrosol ($n = 0.37$); ●: 1% CMC ($n = 0.42$); ▲: 1% Natrolsol ($n = 0.56$); ▼ 0.14% CMC ($n = 0.58$); +: 0.28% CMC ($n = 0.57$); ♦: water. Open symbols: data due to Dyster et al. (1993); closed symbols: data due to Koutsakos and Nienow (1990).

($Re < 40 - 60$) and a gradual increase in the transition regime ($40 - 60 < Re < 10^4$). In the turbulent regime, Fl has a constant value of about 0.78. In the laminar regime, Fl is about one order of magnitude smaller for shear-thinning liquids than for Newtonian liquids, but Fl increases much faster with Re. The experiment with 1% CMC (Koutsakos and Nienow, 1990) revealed that at $Re \approx 10$ a so-called cavern is formed around the impeller. The cavern is characterised by a steep decrease of the radial velocity, which even becomes negative (i.e. flow towards the impeller) at positions $r/R > 1.2$. This clearly has an impact on the pumping capacity of the impeller, and explains why the Flow numbers are so small in the laminar regime. The two curves approach one another in the turbulent regime, but the data due to Koutsakos and Nienow (1990) were in the range $Re < 10^3$ only.

Note that three of the five fluids investigated by Koutsakos and Nienow (1990) had essentially the same flow index ($n = 0.57$). This partly supports the intuitive idea that a family of curves must exist (one for each value of n) if the shear-thinning character of the fluid is of importance. Measurements in the laminar regime (Dyster et al., 1993) are consistent with the finding due to Norwood and Metzner (1960) that discharge rates from a Rushton turbine in Newtonian liquids scale with $\sqrt{\rho/\mu}$.

The Flow numbers reported in this paper are shown in Fig. 11. In our experiments, the Flow numbers found for the shear-thinning liquids are somewhat lower than for Newtonian liquids. A small increase with increasing Re is visible, but not as pronounced as found by Koutsakos and Nienow (1990). Overall, the Fl-data are more in line with the findings due to Dyster et al. (1993) and this raises some questions as to the data reported by Koutsakos and Nienow (1990). The most logi-

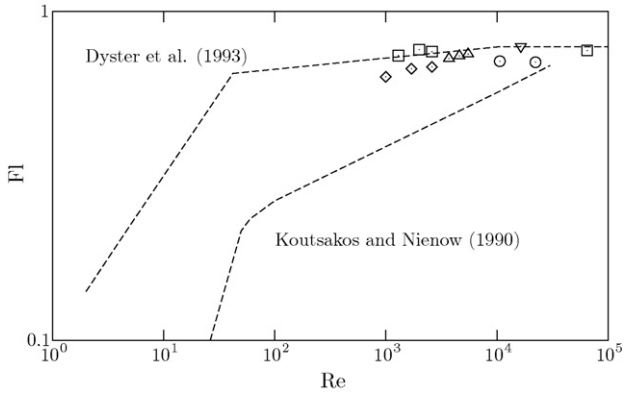

Fig. 11 – Flow number as a function of the Reynolds number, own data reported in this paper compared to the literature data of Fig. 10. □: Newtonian fluids, $n = 1.0$; ⊙: 0.1% Blanose (b), $n = 0.85$; △: 0.1% Blanose (a), $n = 0.77$; ▽: 0.05% Keltrol, $n = 0.71$; ◇: 0.2% Blanose, $n = 0.68$.

cal explanation is that the fluids used by the latter authors are not just shear-thinning, but also show visco-elastic behaviour. The primary normal stress difference in those fluids may cause an inwards directed flow near to the impeller, which reduces partly the inertia driven outflow, resulting in lower Flow numbers (Özcan Taskin, 1993). Power curves of the fluids showed an increased power consumption in the laminar regime. This effect was also found by Nienow et al. (1983) and attributed to visco-elasticity of the fluids.

4.3. *RMS velocities*

The dominant effect of the trailing vortices on the turbulence intensities is very well seen in the profiles of the rms velocities in the impeller discharge domain. The results of the measurements are presented in Fig. 12. For the *radial* and *tangential* component, the largest effect of the vortices is found at $z^* = 0$, while for the *axial* component it is found near $z^* = \pm 0.5$. A second maximum both below and above the impeller plane is found for the radial component at $|z^*| = 0.5 - 1$. The bell-shaped curve through the tangential rms data is narrower than the curve for the mean tangential velocities in Fig. 9(c). Our data look very similar to those reported by Wu and Patterson (1989); the numerical values found for the non-dimensional velocities in our measurements, however, are higher than those reported by Wu and Patterson (1989).

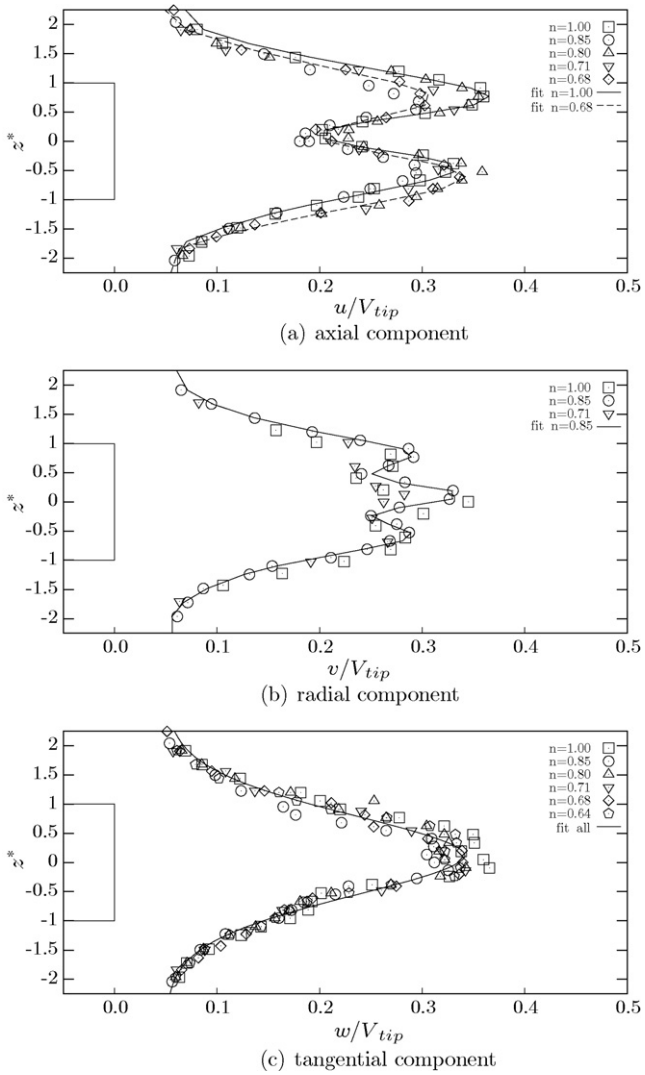

Fig. 12 – Profiles of rms velocities for all fluids at their highest Reynolds number in the impeller discharge domain. (a) Axial component, (b) radial component, (c) tangential component.

For reasons of completeness, we have tested several polynomial curves in the program TableCurve 2D to represent the complicated profiles of the axial and radial velocity component. Admittedly, using polynomials in fitting data has some drawbacks, but nevertheless they offer the simplest way to communicate our data. The resulting polynomial curves are

Table 12 – Results non-parametric tests for the total rms velocity fits (impeller outflow).

Profile	Parameter	$t_{.05}$	$t(n)$	$t(Re)$	Significant-n	Significant-Re
Axial velocity	u_0	1.943	−0.09	1.47	no	no
	z_0	1.943	−0.52	−0.08	no	no
	Max @ neg.z^*	1.943	0.18	0.16	no	no
	Max @ pos.z^*	1.943	1.97	2.29	yes	yes
	Width @ max.	1.943	−3.77	−2.34	yes	yes
	Width @ $u = 0.1$	1.943	−0.26	0.07	no	no
Radial velocity	v_0	1.796	4.46	2.00	yes	yes
	z_0	1.796	1.63	1.18	no	no
	Width @ $v = 0.15$	1.796	1.84	6.86	yes	yes
Tangential velocity	w_0	1.812	0.63	0.82	no	no
	w_∞	1.812	−1.06	−2.39	no	yes
	z_0	1.812	0.44	0.43	no	no
	Width @ $w = 0.15$	1.812	0.46	1.70	no	no

as follows:

$$u^*_{tot} = \max\left[u_\infty; \frac{u_0 + a(z^* - z_0)^2 + b(z^* - z_0)^4}{1 + c(z^* - z_0)^2 + d(z^* - z_0)^3 + e(z^* - z_0)^4}\right] \quad (25)$$

$$v^*_{tot} = \max\left[v_\infty; \frac{v_0 + a(z^* - z_0)^2 + b(z^* - z_0)^4}{1 + c(z^* - z_0)^2 + d(z^* - z_0)^4 + e(z^* - z_0)^6}\right] \quad (26)$$

$$w^*_{tot} = w_\infty + (w_0 - w_\infty)\exp\left[-C \cdot \left|z^* - z_0\right|^m\right] \quad (27)$$

As indicated by the non-parametric test results presented in Table 12, both the flow index and the Reynolds number have a pronounced effect on the axial and radial components of the total rms velocity (as judged with the help of some characteristic points of the curves). Only a small *Re*-effect was found for the tangential rms velocity far away from the impeller (w_∞). Ignoring the latter effect, all tangential rms data could be described by means of a single curve:

$$w^*_{tot} = 0.050 + (0.342 - 0.050)\exp\left[-0.916 \cdot \left|z^* - 0.12\right|^{1.79}\right] \quad (28)$$

5. Conclusions

The central issue in this paper was the question whether or not, and if so that what extent, turbulent flow of shear-thinning liquids in stirred vessels provided with baffles is different from turbulent flow of Newtonian liquids under similar conditions. In other words: do the non-Newtonian fluid properties still have an impact on the turbulent flow characteristics induced by, more in particular, a Rushton turbine in a vessel provided with baffles. In fact, the question is beyond which Reynolds number the turbulent flow field exhibits Reynolds number similarity in all parts of a stirred vessel filled with a shear-thinning liquid.

The approach pursued in the investigation reported in this paper was to measure at various positions in the vessel the three components of the mean and fluctuating velocity field by means of Laser-Doppler Anemometry (LDA). Care was taken to exclude the effect of particularly velocity bias on the measured quantities. The flow in the impeller discharge region was characterised by phase-averaged profiles along the impeller blade tip and at the level of the impeller disc center-line. The number of data points in each profile was considerably increased, compared to previous work, in order to capture the flow field in greater detail and to improve existing correlations.

Although the majority of the experiments were supposedly performed in the turbulent regime, in some cases an effect of *Re* on the profiles was still found in the measurement data. In some cases, the flow index had an effect as well. The absence or presence of a dependency on *Re* and/or *n* was tested with the help of Spearman's rank-order correlation coefficient. This is a non-parametric test detecting the likelihood of a dependency only. The results obtained with this method are summarised as follows:

- At the level of the impeller disc: the radial profile of the mean axial velocity exhibits a dependency on *Re* between $r/R = 1.0$ and $r/R \approx 2.0$, while the flow index does not have an effect on this profile. The mean radial and tangential velocity components are independent of both Reynolds number and flow index.
- The flow index has a widening effect on the discharge profiles of V/V_{tip} and W/V_{tip}. This results in slightly lower Flow numbers for the shear-thinning solutions, although not as pronounced as found by Koutsakos and Nienow (1990). A stronger effect of the Reynolds number is also found for the width of the discharge profile of the radial velocity.
- Both *Re* and *n* have an effect on the fluctuating tangential velocity *w* at $r/R = 1.0$.
- As to the discharge profiles, both *Re* and *n* have a pronounced influence on the various characteristic points in the profiles of the axial and radial velocity component. Only the tangential component can be described with a single fit relation for all fluids.
- In most cases, a deviating behaviour of the 0.1 wt% Blanose solution with $n = 0.85$ is found. As the reason for this is unclear, these measurements were ignored in determining the overall fits.

In the cases that both the Reynolds number and the flow index have a statistically significant effect on the various velocity profiles and on the exact position of so-called characteristic points of these profiles, the effects may be not independent because, for the fluids used, low values of *n* are associated with low values of *Re*, and vice versa. In addition, *n* occurs in the Metzner–Otto definition of the Reynolds number.

The overall conclusion is that Reynolds number similarity was not observed under all experimental conditions. Remarkably, the shear-thinning property of the fluids was found to have a different impact on the various velocity components. The data presented provide an impetus to study in greater detail how exactly non-Newtonian liquid properties affect the flow structure under close-to-turbulent conditions. Since in shear-thinning liquids the effective liquid viscosity depends on the (local) shear rate with the flow structure being strongly 3D, the state of Reynolds number similarity may not be attained at all positions and for all velocity components simultaneously when impeller speed (and hence Reynolds number) is increased.

Anyhow, several empirical correlations have been presented for the various velocity components reflecting the effects – if present – of Reynolds number and flow index. These correlations are claimed to apply throughout within the ranges of Reynolds numbers *Re* and flow indices *n* investigated. As such, they provide easy validation material for Computational Fluid Dynamics (CFD) simulations for stirred vessels filled with shear-thinning liquids, equipped with a Rushton impeller and with baffles, and operated under (close to) turbulent flow conditions, even in cases not exactly investigated in the experiments reported here. Of course, these correlations should not be used outside the ranges of *Re* and *n* investigated.

Additional information

An Excel-file has been prepared which includes the correlation fits of all profiles for all experiments described in this paper and also for the periodic and the fully turbulent contributions to the rms velocity fluctuations. This Excel file can be obtained from the corresponding author free of charge. More data and plots can also be found in Venneker (1999).

Acknowledgment

This work was supported by the Chemical Sciences (CW) Division of the Netherlands Organisation for Scientific Research (NWO) with financial aid from the Netherlands Technology Foundation (STW).

References

Adams, L.W. and Barigou, M., 2007, CFD analysis of caverns and pseudo-caverns developed during mixing of non-Newtonian fluids. Chem. Eng. Res. Des., 85: 598–604.

Arratia, P.E., Kukura, J., Lacombe, J. and Muzzio, F., 2006, Mixing of shear-thinning fluids with yield stress in stirred tanks. AIChE J., 52: 2310–2322.

Bakker, A., 1992, Hydrodynamics of stirred gas–liquid dispersions. Ph.D. Thesis, Delft University of Technology.

Bakker, A. and Van den Akker, H.E.A., 1994, Single-phase flow in stirred reactors. Chem. Eng. Res. Des., 72: 583–593.

Couerbe, G., Fletcher, D.F., Xuereb, C. and Poux, M., 2008, Impact of thixotropy on flow patterns induced in a stirred tank: numerical and experimental studies. Chem. Eng. Res. Des., 86: 545–553.

Drain, L.E., (1980). *The Laser Doppler technique*. (Wiley).

Durst, F., Melling, A. and Whitelaw, J.H., (1976). *Principles and Practice of Laser-Doppler Anemometry*. (Academic Press).

Dyster, K.N., Koutsakos, E., Jaworski, Z. and Nienow, A.W., 1993, A LDA study of the radial discharge velocities generated by a Rushton turbine: Newtonian fluids. Chem. Eng. Res. Des., 71: 11–23.

Fangary, Y.S., Barigou, M., Seville, J.P.K. and Parker, D.J., 2000, Fluid trajectories in a stirred vessel of non-Newtonian liquid using positron emission particle tracking. Chem. Eng. Sci., 55: 5969–5979.

Hinze, J.O., (1959). *Turbulence. An Introduction to its Mechanism and Theory*. (McGraw-Hill).

Koutsakos, E., Nienow, A.W., 1990, Effects of rheological properties of simulated fermentation broths on flows in stirred bioreactors: a Laser Anemometry study, in Rheology of Food, Pharmaceutical and Biological Materials with General Rheology, Carter, R.E. (ed), pp. 284–302.

Koutsakos, E., Nienow, A.W. and Dyster, K.N., 1990, Laser Anemometry study of shear thinning fluids agitated by a Rushton turbine, In *IChemE Symp. Series No. 121* , pp. 51–73.

Lunden, M., 1995, Simulation of three-dimensional flow in stirred vessels: influence of the impeller-modeling and scale-up. Chem. Eng. Commun., 139: 79–114.

Metzner, A.B. and Otto, R.E., 1957, Agitation of non-Newtonian fluids. AIChE J., 3: 3–10.

Mishra, V.P. and Joshi, J.B., 1993, Flow generated by a disc turbine. Part III. Effect of impeller diameter, impeller location and comparison with other radial flow turbines. Chem. Eng. Res. Des., 71: 563–573.

Nienow, A.W., Wisdom, D.J., Solomon, J., Machon, V. and Vlcek, J., 1983, The effect of rheological complexities on power consumption in an aerated, agitated vessel. Chem. Eng. Commun., 19: 273–293.

Norwood, K.W. and Metzner, A.B., 1960, Flow patterns and mixing rates in agitated vessels. AIChE J., 6: 432–437.

Nouri, J.M. and Hockey, R.M., 1998, Power number correlation between Newtonian and non-Newtonian fluids in a mixing vessel. J. Chem. Eng. Jpn., 31: 848–852.

Nouri, J.M. and Hockey, R.M., 2008, Flow characteristics of Newtonian and non-Newtonian fluids in a vessel stirred by a 60° pitched blade impeller. Int. J. Multiphys., 2: 83–105.

Nouri, J.M. and Whitelaw, J.H., 1990, Flow characteristics of stirred reactors with Newtonian and non-Newtonian fluids. AIChE J., 36: 627–629.

Nouri, J.M., Whitelaw, J.H. and Yianneskis, M., 1987, The scaling of the flow field with impeller size and rotational speed in a stirred reactor, In *2nd Int. Conf. on Laser Anemometry – Advances and Applications* , pp. 489–500.

Özcan Taskin, N.G., 1993, On the effects of viscoelasticity in stirred tanks. Ph.D. Thesis, University of Birmingham.

Paul, E.L., Atiemo-Obeng, V.A., & Kresta, S.M. (eds) 2004, *Handbook of Industrial Mixing. Science and Practice*. (Wiley).

Sheskin, D.J., (1997). *Handbook of parametric and nonparametric statistical procedures*. (CRC Press).

Skelland, A.H.P., (1967). *Non-Newtonian Flow and Heat Transfer*. (Wiley).

Szoplik, J. and Karcz, J., 2008, Mixing time of a non-Newtonian liquid in an unbaffled agitated vessel with an eccentric propeller. Chem. Papers, 62: 70–77.

Tatterson, G.B., (1991). *Fluid mixing and gas dispersion in agitated tanks*. (McGraw-Hill).

Tennekes, H. and Lumley, J.L., (1972). *A first course in turbulence*. (MIT Press).

Townsend, A.A., (1956). *The structure of turbulent shear flow*. (Cambridge University Press).

Van den Akker, H.E.A., 2006, The details of turbulent mixing processes and their simulation. Adv. Chem. Eng., 31: 151–229.

Van der Molen, K. and Van Maanen, H.R.E., 1978, Laser-Doppler measurements of the turbulent flow in stirred vessels to establish scaling rules. Chem. Eng. Sci., 33: 1161–1168.

Venneker, B.C.H., 1999, Turbulent flow and gas dispersion in stirred vessels with pseudo-plastic liquids. Ph.D. Thesis, Delft University of Technology.

Wu, H. and Patterson, G.K., 1989, Laser-Doppler measurements of turbulent-flow parameters in a stirred mixer. Chem. Eng. Sci., 44: 2207–2221.

Yianneskis, M., Popiolek, Z. and Whitelaw, J.H., 1987, An experimental study of the steady and unsteady flow characteristics of stirred reactors. J. Fluid Mech., 175: 537–555.